Measurement 203 (2022) 111965

Contents lists available at ScienceDirect

Measurement

journal homepage: www.elsevier.com/locate/measurement

Image signal denoising method of grating linear displacement sensor based on NLM

Xu Gao [a,b], Xuebin Zhang [c], Kaiwei Li [d,*], Pengfei Wang [e]

[a] School of OPTO-Electronic Engineering, Changchun University of Science and Technology, Changchun 130022, China
[b] State Key Laboratory of Applied Optics, Changchun 130022, China
[c] School of OPTO-Electronic Engineering, Changchun University of Science and Technology, Changchun 130022, China
[d] Key Laboratory of Bionic Engineering of Ministry of Education, Jilin University, Changchun 130022, China
[e] School of OPTO-Electronic Engineering, Changchun University of Science and Technology, Changchun 130022, China

ARTICLE INFO

Keywords:
Terms—Grating
Displacement measurement
Image
Cascade stripe
Denoising
Inverse ratio kernel NLM

ABSTRACT

To improve the measurement resolution and accuracy of the grating displacement sensor, this paper proposes an image signal denoising method of grating linear displacement sensors based on NLM. Firstly, the optical system is designed to load the displacement information into the fringe image based on the grating pitch; Then, the principle of NLM image denoising is studied, and the inverse ratio kernel NLM denoising algorithm is designed; Thirdly, the effect of denoising algorithm is compared with the typical kernel function; Finally, the optimized image is used for displacement demodulation. The experimental results show that the SNR of the image is 30.1370db after denoising by this algorithm, and the high-precision displacement stage is set at 20 nm, 40 nm, and, 60 nm. Using the method in this paper, the positioning can be calculated to 22.7 nm, 38.2 nm, and 63.3 nm, and the sub-pixel positioning of the image and the nanopositioning measurement of the displacement are completed.

1. Introduction

The grating pitch is taken the measurement standard of the displacement measurement system based on diffraction grating, This has the advantages of strong anti-interference and high precision. The classical grating measurement system uses sine waves for displacement demodulation. However, due to the problems of a large volume of split-term optical paths, large phase edge demodulation errors, limited sub-division resolution, and the continuous progress of image detector technology levels, the resolution of measurement systems based on image signal detection can be improved.

Resolution can be achieved by integrating digital image technology and comprehensively studying precision displacement image processing technology based on diffraction gratings. The demodulation of the displacement image is based on the difference between the images before and after the displacement, and uses digital image processing technology to calculate the displacement of the target object in the image. It is necessary to denoise the fringe before beginning fringe image demodulation in order to obtain higher resolution.

At present, there are few effective denoising algorithms for image background diffraction shading, and these have been improved on the basis of frequency-domain low-pass filtering theory [1–6]. Examples include the work of Lucas and Kanade, and Horn and Schunck. The L-K optical flow algorithm and H-S optical flow algorithm were proposed respectively [7,8], with the optical flow constraint equation. Simon Baker et al. created an optical flow method database. Furthermore, from the grating engraving coding itself, Lili Qi of the Changchun Institute of Optics, Precision Mechanics and Physics at the Chinese Academy of Sciences proposed the angular displacement measurement technology of an image encoder based on single-circle coding imaging [9,10]. A two-dimensional gold matrix method based on a two-dimensional spatial coding mode was proposed by the Shanghai Institute of Optoelectronics and University of Chinese Academy of Sciences [11]. This method demodulates the two-dimensional image displacement. NASA studied coding technology, which is based on image processing technology. High-resolution, high-sensitivity linear displacement and angular displacement absolute encoders have been developed [12]-[13]. After continuous innovation and improvement, the angular displacement resolution of the proposed encoders can reach 0.01 s, and the linear displacement resolution can reach 0.01 μm. Yu Hai proposed a lensless

* Corresponding author at: School of OPTO-Electronic Engineering, Changchun University of Science and Technology, Changchun 130022, China.
E-mail addresses: gaox19870513@163.com (X. Gao), kaiwei_li@jlu.edu.cn (K. Li).

https://doi.org/10.1016/j.measurement.2022.111965
Received 12 July 2022; Received in revised form 2 September 2022; Accepted 15 September 2022
Available online 22 September 2022
0263-2241/

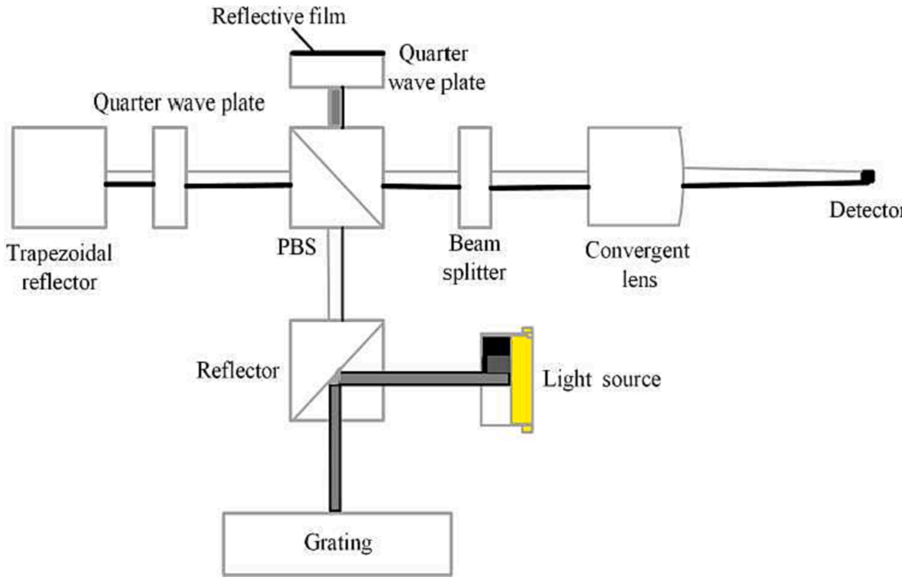

Fig. 1. Schematic diagram of grating image displacement imaging system.

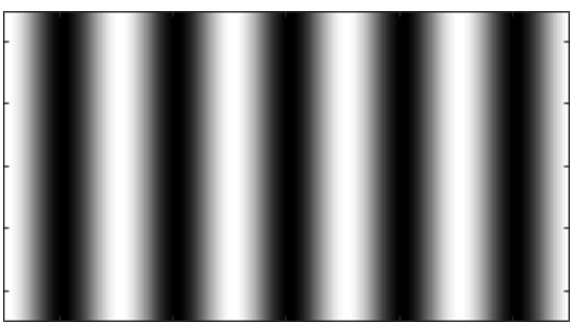

Fig. 2. Virtual moire fringe simulation image.

LDM image optical path image linear displacement encoder to reduce the device volume[14].

These are analyzed in this paper, aiming at the noise caused by optical devices and the acquisition of fringe images. Based on the analysis of the image fringes' characteristics of grayscale continuity and global periodic structure, and compared with the current newer BM3D denoising algorithm (Block-matching and 3D Filtering) [15], a nonlocal means (NLM) denoising algorithm suitable for texture and periodic structure denoising is proposed. We focus on the kernel function of the NLM denoising algorithm, design an inverse proportional kernel function, and propose an inverse proportional kernel NLM denoising algorithm that can effectively denoise the fringe image.

2. Displacement image optical sensing system

The displacement measurement system based on diffraction grating loads the microdisplacement information into the fringe image through the optical sensing system and converts it into a sine wave or image signal by CCD or CMOS. When the measured system moves with the grating, the displacement information is reflected in each parameter of the presented photoelectric signal, and the dynamic changes and motion characteristics are reflected in the photoelectric signal in the displacement measurement. The signal parameters are accurately demodulated through the photoelectric signal demodulation method, and then the position information of the tested system is retrieved, as shown in Fig. 1.

In the optical path, the wavelength of the laser light source is 632.8 nm, the number of grating lines is 1200 lines/mm, and the fast axis direction of Q1 and Q2 forms a 45° angle with the horizontal. The light source emits a monochromatic laser, which is vertically injected into the grating through the refractive mirror. This occurs according to the diffraction of the incident light perpendicular to the grating:

$$d\sin\theta = m\lambda \tag{1}$$

The calculation shows that the 1200-lines/mm grating emits ±1 order diffracted light, and the diffracted beam passes through the refractive mirror again and is vertically incident into the polarization splitting prism (PBS). Due to the symmetry of the optical path, the $+1$ order diffracted light is introduced as an example. After the first-order diffracted light passes through PBS, the reflected light component passes through a quarter wave plate, and the polarization state changes from linearly polarized (S) light to circularly polarized light. Then, it passes through the trapezoidal reflector and coincides with the optical path of the reflection component of the -1 order diffracted light. After passing through a quarter-wave plate, the polarization state is changed into linear polarization (P) light, which enters the birefringent crystal after passing through the polarization splitting prism (PBS). After the transmitted light component passes through the quarter-wave plate, it is reflected by the mirror and passes through the quarter-wave plate again. The polarization state changes from linear polarization (P) to linear polarization (S), and the vibration direction changes. After passing through PBS, it is reflected into the birefringent crystal.

Similarly, the transmitted and reflected light components of -1 diffraction light enter the birefringent crystal after passing through the optical system. The birefringent crystal element separates two beams of light with different overlapping polarization states in parallel so that there is a small difference in the distance between two symmetrical groups of light with the same polarization state in the optical path. After passing through the converging lens, the four beams intersect in the detection plane, in which two groups of light with the same polarization interfere to form two groups of interference fringes, and the two groups of fringes are further superimposed to form a virtual stacked fringe.

According to the diffraction interference principle and grating equation, the virtual stacked grating fringe signal is obtained as:

$$I^{'} = 4I\cos[4n\pi x(D_1 - D_2)/D_1D_2] \tag{2}$$

where I is the intensity of diffracted light, D_1 and D_2 are the interference fringe periods before and after grating movement, n is the diffraction order, and x is the grating displacement. The virtual stacked fringe

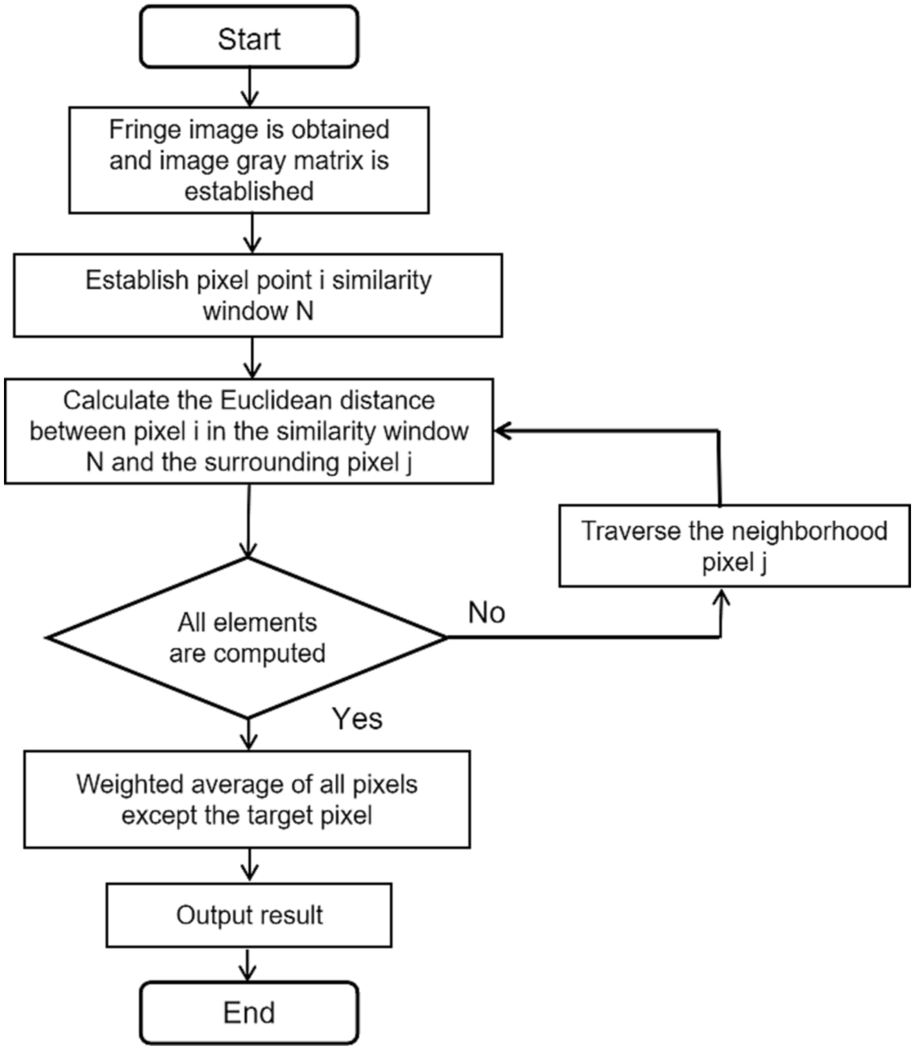

Fig. 3. Improved NLM algorithm flow chart.

signal is in the form of trigonometric function, as shown in Fig. 2.

3. Denoising algorithm of grating displacement interference fringe signal based on NLM

3.1. Design of improved non-local mean (NLM) denoising method

Assuming local regularity and following the principle of neighborhood filtering, Buades et al. proposed a nonlocal means (NLM) denoising algorithm [1,17]. This algorithm uses the information of the fixed-size window around the pixel to represent the characteristics of the target pixel in order to use the structural similarity to define the differences between pixels. This protects the structural information of the image and achieves a better denoising effect. The algorithm flow chart is shown in Fig. 3.

Specifically, the nonlocal mean algorithm means that in a discrete noise image Z defined in a bounded region, for a pixel i, the weighted average of the pixels of the entire image is used to calculate the estimated target point called $NL(z)(i)$ according to (3). We use the weighted average of the pixels of the entire image to calculate the estimated target point $NL(z)(i)$.

$$NL(z)(i) = \sum_j \omega(i,j)z(j)$$

$$C(i) = \exp^{\left(\frac{-d(i,j)}{h^2}\right)}$$

$$d(i,j) = ||z(N_i) - z(N_j)||^2_{2a} \tag{3}$$

where ω is the weight, satisfying $0 \leq \omega(i,j) \leq 1, \sum_j \omega(i,j) = 1$.

To compare the image similarity, the neighborhood system N is defined as the subset of the image domain, and the pixel $i \in N$ in the image, where N is called the neighborhood or similarity window of pixel i. The window in this paper selects the square for calculation. The similarity of gray values between pixels i and j determines their similarity, and pixels with high similarity are given greater weight in the process of weighted averaging. In contrast, pixels with low similarity are given smaller weights in the process of weighted averaging.

The similarity between pixels is used to determine the weight given by the algorithm and to quantitatively calculate the similarity between pixels. The Euclidean distance is selected for similarity characterization. At the corresponding position between the noise image and the original noise-free image, the Euclidean distance between its vectors satisfies the following relationship:

$$E\left\|z(N_i) - z(N_j)\right\|^a_{2,a} = \left\|y(N_i) - y(N_j)\right\|^a_{2,a} + 2\sigma^2 \tag{4}$$

where z and y represent the noisy image and the original noiseless image, respectively, and σ^2 is the noise variance. The formula represents

Table 1
Typical kernel functions.

Name	Expression
exponential	$f(x) = \exp\left(\frac{-x}{\lambda^2}\right)$
cosine	$f(x) = \begin{cases} \cos(\frac{\pi x}{2\lambda}) & 0 < x \leqslant \lambda \\ 0 & else \end{cases}$
Gaussian	$f(x) = \exp\left(\frac{-x^2}{2\lambda^2}\right) \quad x > 0$
Turkey	$f(x) = \begin{cases} \frac{1}{2}\left(1 - \left(\frac{x}{\lambda}\right)^2\right)^2 & 0 < x \leqslant \lambda \\ 0 & else \end{cases}$
wave	$f(x) = \begin{cases} \frac{\sin(\pi x/\lambda)}{\pi x \lambda} & 0 < x \leqslant \lambda \\ 0 & else \end{cases}$

the grayscale of the noisy image.Compared with the Euclidean distance of the original image, the Euclidean distance calculated maintains the similarity between pixels. In the noisy image, pixels similar to pixel i are also considered to be similar to pixel i in the original image. Based on the Euclidean distance defined above, the weight between pixels i and j is defined as follows:

$$\omega(i,j) = \frac{1}{Z(i)}\exp(-\|z(N_i) - z(N_j)\|_{2,a}^2/h^2)$$

where $Z(i) = \sum_j exp(-\|z(N_i) - z(N_j)\|_{2,a}^2/h^2)$ is the normalization constant, and h is the decay rate of the exponential function. The traditional weight function adopts the form of an exponential function with fast attenuation speed. The exponential form can give different weights according to different European distances.

Noise can be removed by a nonlocal mean algorithm with the property of repeated structure in the image. This is especially suitable for images with periodic structure and texture structure, and can improve the quality of the image and preserve the details and edges of the image.

3.2. Kernel function design of NLM denoising algorithm

The weights of the NLM image denoising algorithm in the process of weighted averaging need to be calculated by a weighted kernel function (hereafter referred to as the “kernel function”). Therefore, the selection of a weighted kernel function for weight calculation is important.

The traditional kernel functions include exponential, cosine, Gaussian, Tukey, and wave kernel, as shown in Table 1.

Among the above five kernel functions, the Gaussian kernel function is the most classical robust radial basis function and has good anti-interference ability to noise. Its scope of action is determined by the set parameters. If it exceeds the set scope, then it will have no impact on the data. The exponential kernel function is essentially a variant of the Gaussian kernel function. Compared with the Gaussian kernel function, the exponential kernel function reduces the influence of parameters on its calculation results by adjusting the distance between vectors, but the action range is also reduced. The cosine kernel function can map the original data to the high-dimensional space related to the angle and can better express the relationship between two variables. Turkey is often overweighted, the wave kernel function is mostly used in audio processing, and the processing of image signals still needs to be improved.

3.3. Proposal and design of inverse ratio kernel NLM denoising algorithm

If the number of image pixels is N, set the search window size D × D. Neighborhood window size d × d. The image block distance is:

$$s_t(z) = \|v(z) - v(z+t)\|_2^2 \tag{6}$$

where, $t = y - x \in [| - D_s + D_s|]^2$ is a translation vector, the Euclidean distance formula (7) can be obtained.

To design a weight kernel function that is more suitable for the fringe image denoising generated by the grating displacement image detection system, the similarity weight allocation performance of different kernel functions for the fringe image is analyzed and compared.

The Euclidean distance is used to represent the similarity of images. Combined with the following Euclidean distance formula, the traditional exponential, Gaussian, and Tukey kernel functions are analyzed.

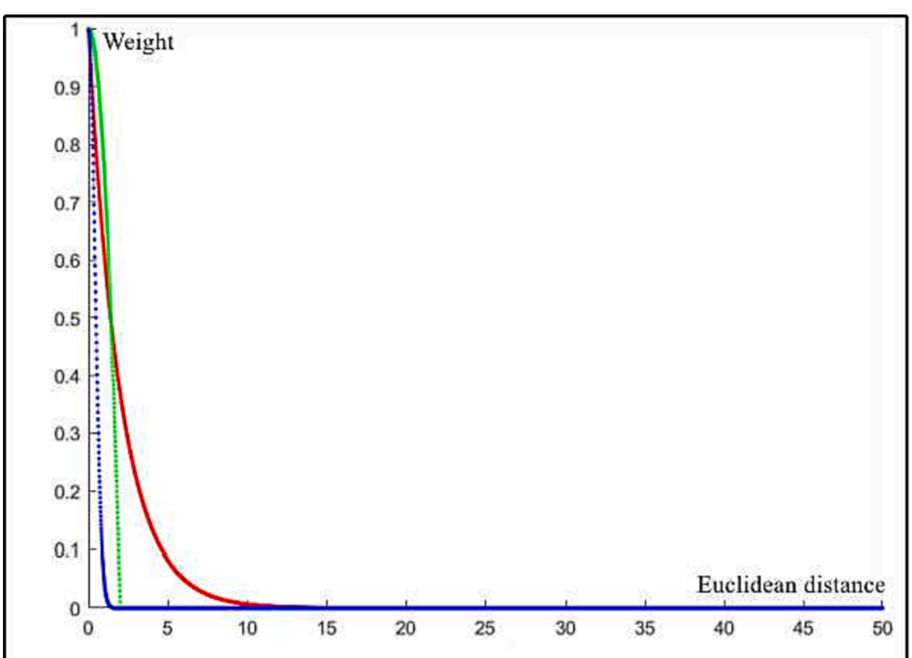

Fig. 4. Weights -Euclidean distance curve of traditional kernel functions.

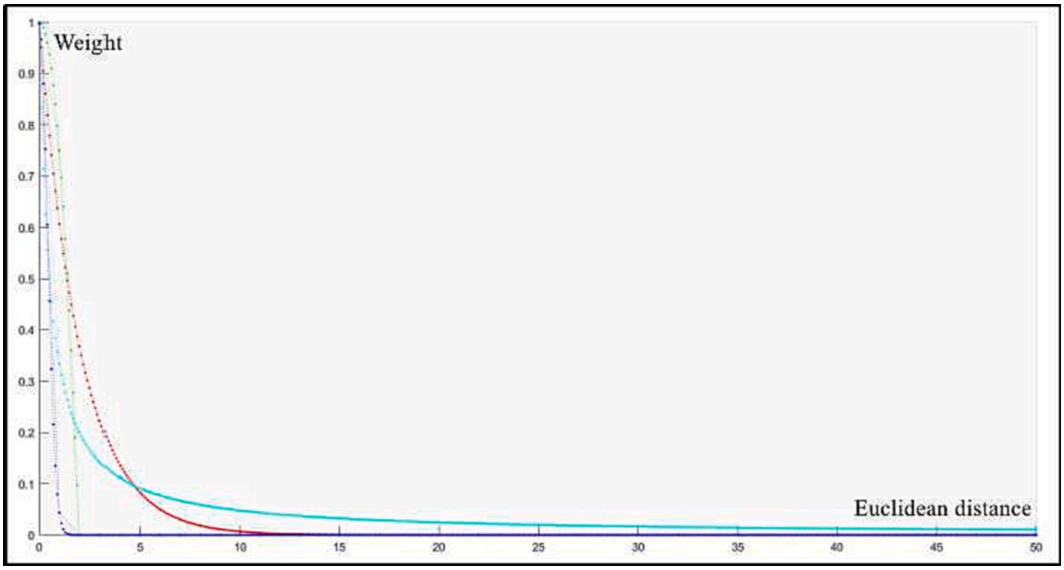

Fig. 5. Weight-Euclidean distance curve.

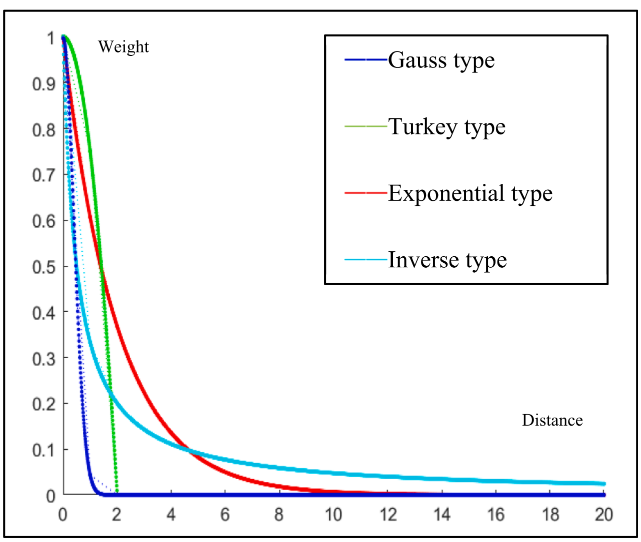

Fig. 6. Weight-Euclidean distance curve(0–20).

$$\|V(x) - V(y)\|_2^2 = \frac{1}{d^2}(S_t(x_1 + d_s, x_2 + d_s) + S_t(x_1 - d_s, x_2 - d_s) - S_t(x_1 + d_s, x_2 - d_s) - S_t(x_1 + d_s, x_2 - d_s)) \tag{7}$$

Taking the fringe image as the denoising object, the weight Euclidean distance curves of the above three kernel functions are drawn, as shown in Fig. 4.

As seen from Fig. 4, in the position where the Euclidean distance value is greater than 10 and the image similarity is low, the weight allocation values are almost all 0, and there is no amplitude change. In actual image denoising, there is insufficient weighting that affects the image denoising effect. In a position with a short Euclidean distance and high image similarity, the weight distribution gradient of the exponential kernel function changes less, and the denoising performance is weakened compared with the other two kernel functions.

Therefore, for the fringe image, the purpose is to find a kernel function with an obvious weight gradient change when the Euclidean distance changes to improve the denoising performance of the NLM algorithm for the fringe image.

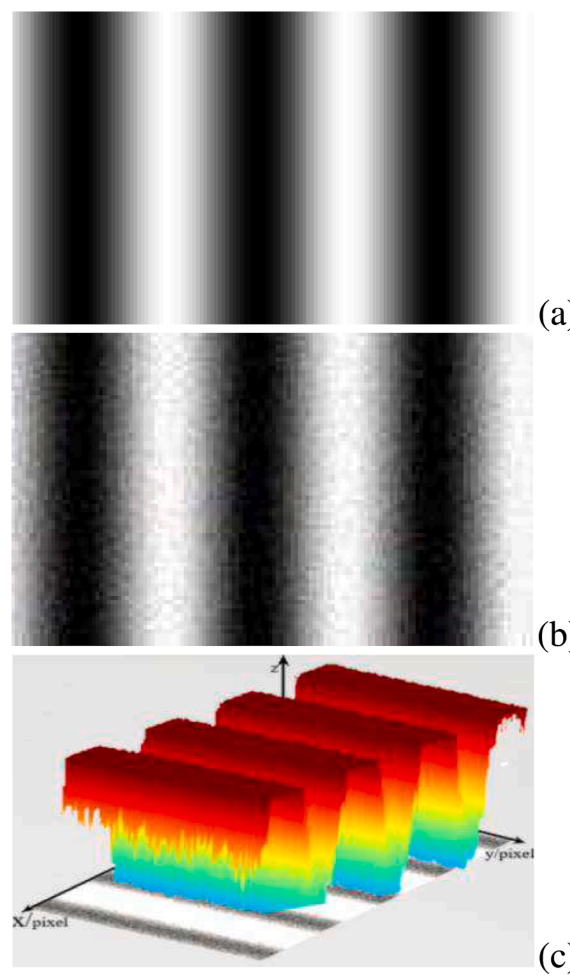

Fig. 7. Simulation of fringe image. (a) No noise. (b) With noise. (c) Gray three-dimensional map (with noise).

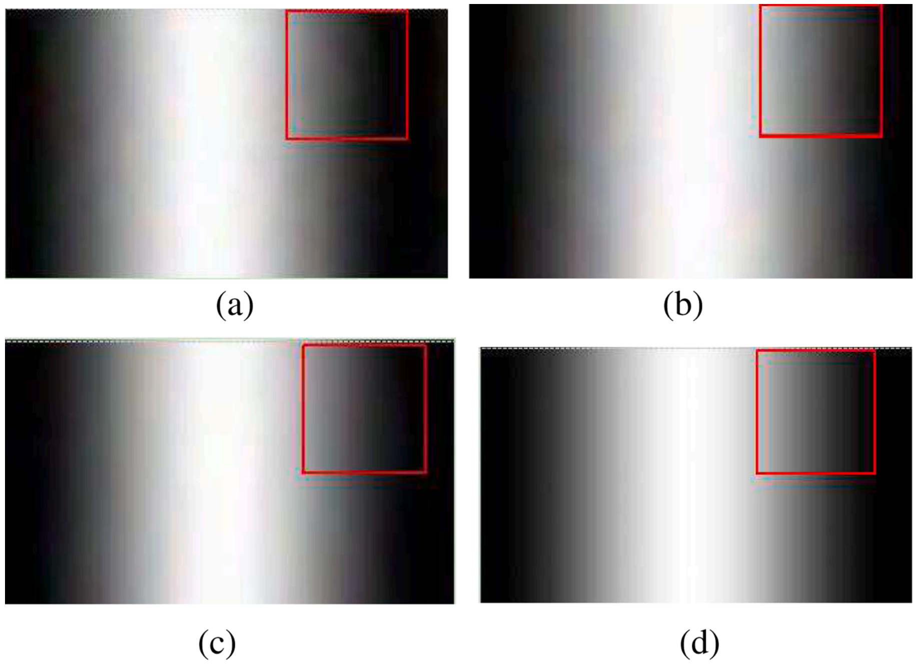

Fig. 8. Comparison of denoising by various kernel functions: (a) Gaussian, (b) Tukey, (c) exponential, and (d) inverse ratio.

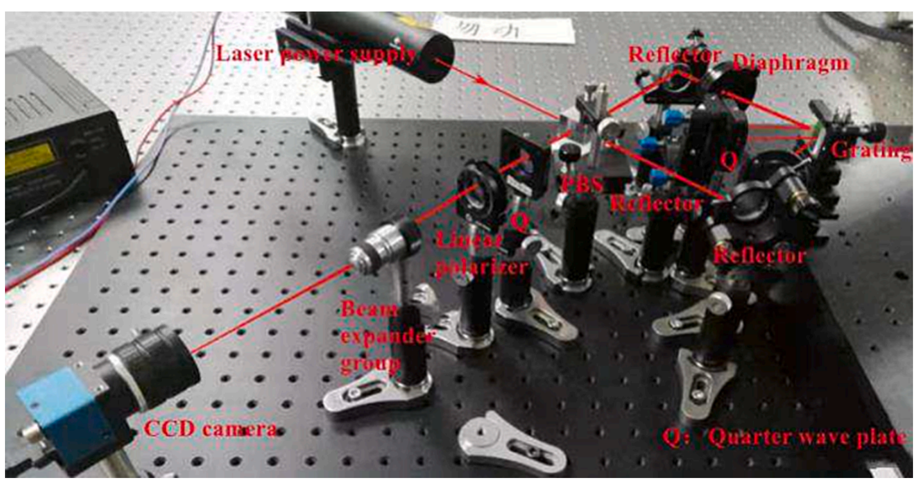

Fig. 9. Experiment of branch debugging.

Table 2
Characteristic parameters of optical components.

Component Name	Type	Name of parameter	Parameter values
Quarter wave plate	ASQW25.4–632.8-4A	Wave length	632.8 nm
		Clear aperture	Φ=25.4 mm
Reflective mirror	OQTMF25.4–400/700	Wavelength range	400–700 nm
		Reflectivity	99.5%
Polarized cube spectroscope	OQPBS-25.4–420-680	Wavelength range	420–680 nm
		Extinction ratio T_p:R_s	>1000

Therefore, an inverse example kernel function[18–21] is proposed in this paper:

$$f(x,y)=\frac{1}{2(2\|x-y\|^2+1)} \tag{8}$$

To verify the correctness of the designed inverse kernel function, the weight Euclidean distance curves of the inverse kernel function proposed in this paper are compared with others, as shown in Fig. 5. To facilitate observation, the image is enlarged between 0 and 20 in Euclidean distance, as shown in Fig. 6.

The dark blue, green, red and light blue curves in the figure represent the weight distribution curves of Gaussian, Turkey, exponential and inverse kernel functions for fringe images respectively. It can be known from the graph that the similarity between the pixel neighborhoods of the curves of Gaussian and Turkey kernel functions is small, that is, when the Euclidean distance is large, the trend is relatively flat. At this time, the distinguishability of the weight is small, and the function weighting is insufficient. Exponential kernel function has no large gradient for weight distribution in the part with high similarity, which

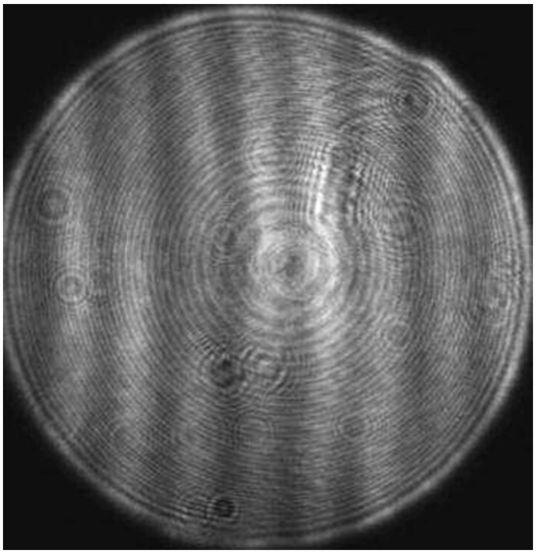

Fig. 10. Image of interference fringes.

Fig. 11. Image of secondary imaging fringe.

means the shorts of the Euclidean distance. The inverse kernel function curve proposed in this paper is shown in light blue in the figure. In the part with high similarity, there is a higher gradient distinction for weight distribution than the exponential kernel function, and in the part with low similarity, there is a more obvious change in weight distribution than the Gaussian and Turkey kernel functions, that is, compared with the traditional kernel function, The inverse kernel function has better gradient and globality for the weight distribution of fringe image.

4. Experiment

4.1. Simulation experiment of stripe image denoising method

4.1.1. Image quality evaluation method

Peak signal to noise ratio (PSNR) is a common method to evaluate image quality. It represents the ratio of the maximum power of the signal to the maximum power of the noise, in decibels (dB). The expression of image peak SNR is shown as (9):

$$PSNR(I,R) = 10 \times \log_{10}\left(\frac{(2^L-1)^2}{MSE(I,R)}\right) \tag{9}$$

L represents the maximum gray level. When evaluating an image using the peak signal-to-noise ratio, the less noise the image contains, the greater the result of the peak signal-to-noise ratio, indicating a higher quality image; conversely, the more noise the image contains, the smaller the result of the peak signal-to-noise ratio, indicating a lower quality image.

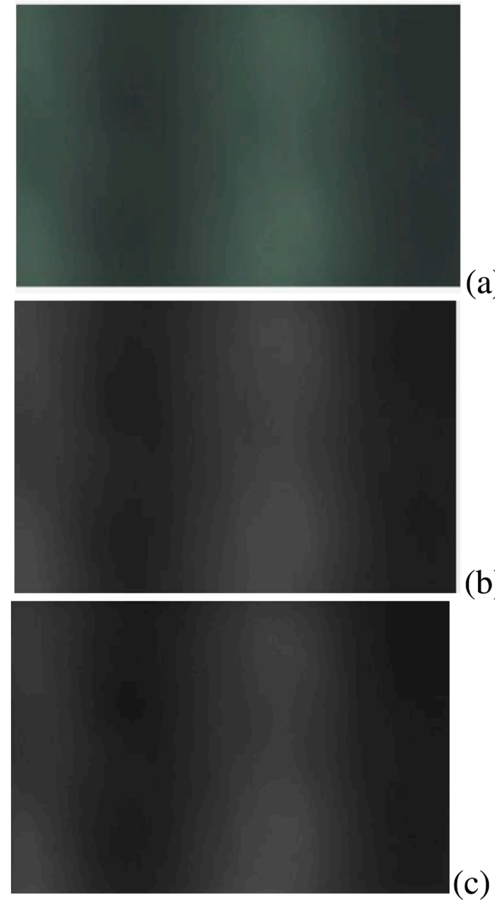

Fig. 12. Image denoising processing. (a) Original figure. (b) Low-pass filter. (c) Denoising of inverse ratio kernel NLM.

4.1.2. Image denoising simulation comparison experiment. The fringe image without noise interference is simulated as shown in Fig. 7(a). The image disturbed by noise is simulated, and 40-dB Gaussian white noise is added to the original image, as shown in Fig. 7(b). To facilitate observation, a three-dimensional gray diagram of the noise image is created, as shown in Fig. 7(c). It is shown that noise has an impact on the quality of the image and reduces the contrast between the image stripes.

Then, the image with noise in Fig. 7(b) is denoised by using the inverse ratio kernel NLM denoising method proposed in this paper and the NLM denoising method of the traditional Gaussian kernel, Tukey kernel, and exponential kernel functions. The image denoised by four different kernel functions is then enlarged, as shown in Fig. 8(a)-(d).

Through direct observation, it can be found that the denoised image is relatively noisy. Fig. 7(b) has been significantly improved, and the fringe contrast is more obvious. In addition, by comparing the fringe edge information in the red box, it can be found that Fig. 8 (d) after denoising by the inverse kernel function NLM method has more obvious boundary information, and Fig. 8(b) for denoising with the Tukey kernel NLM is relatively blurred.

After calculation, the image SNRs after NLM denoising by four different kernel functions are 25.8967 dB, 25.8674 dB, 28.2394 dB, and 30.1370 dB. The peak signal-to-noise ratio calculation results are consistent with the image observation results. In addition, the maximum peak signal-to-noise ratio of the image denoised by the inverse ratio kernel NLM denoising algorithm proposed in this paper is 30.1370 dB through a comparison of the calculated values of the peak signal-to-noise ratio. This is approximately 4.3 dB higher than the minimum value.

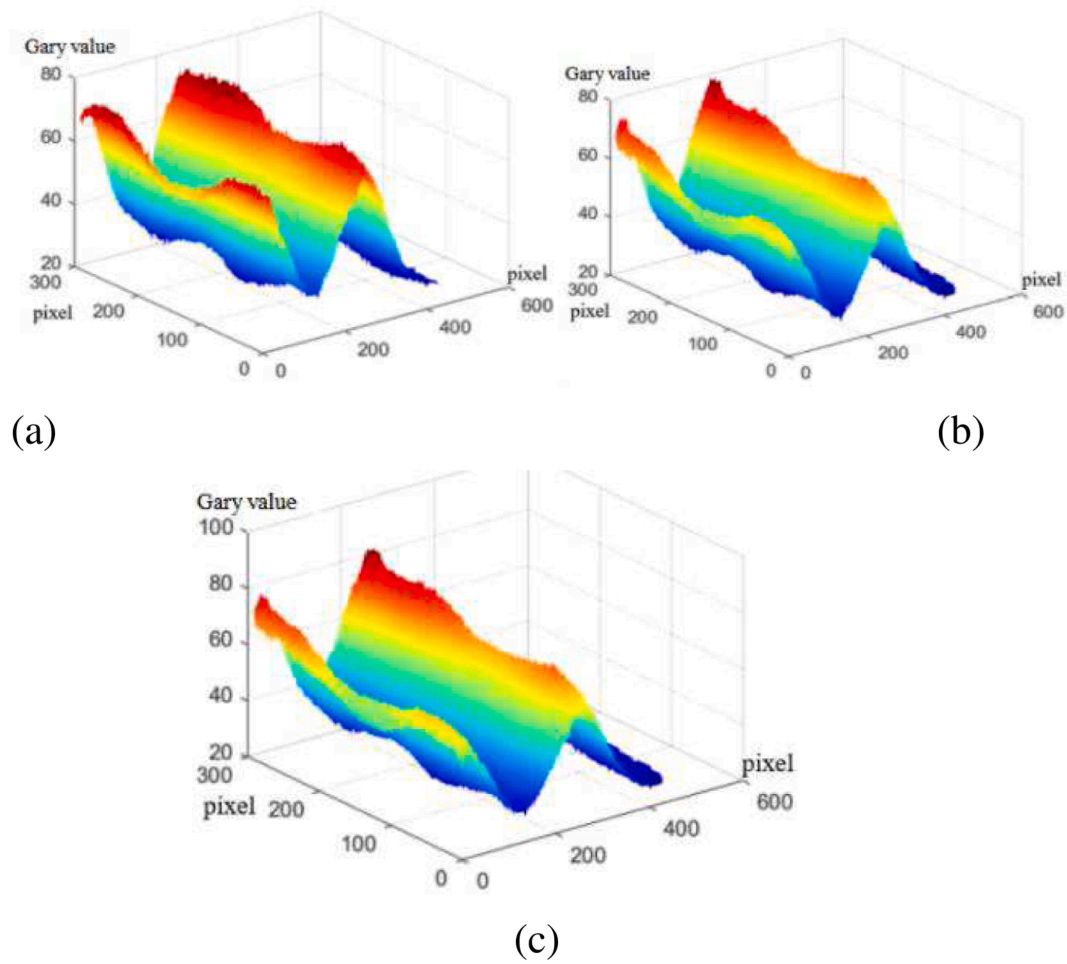

Fig. 13. Gray-value three-dimensional surface graph. (a) Original figure. (b) Low-pass filtering. (c) Inverse ratio kernel NLM denoising.

5. Displacement image measurement effect verification experiment

5.1. System construction and actual interference fringe imaging acquisition

An image displacement measurement system based on diffraction grating is built, as shown in Fig. 9.

The system uses GH25-12 V reflective holographic grating, the grating line density is 1200 lines /mm, corresponding to the grid spacing 833 nm; The CCD of type MER-500-14U3C is used as the image detector; The grating is fixed on the piezoelectric ceramic fretting platform of P-541.2CD; A 632.8 nm laser is used as the light source. In the construction of the optical path, to improve the final imaging quality as much as possible, in the selection of reflection, polarization and other components in the optical path, high reflectivity and transmittance should be selected as much as possible. Table 2 lists some parameters of the components in this experiment.

After actual debugging, the interference fringe image is obtained, as shown in Fig. 10.

From the image, since the system is incident by a laser point light source, parasitic diffraction and interference fringes such as concentric ring shading and small circular spots shown in the figure are generated in the image due to the influence of optical path element defects or unclean and redundant surface reflection. The existence of this noise shading affects the demodulation of subsequent interference fringe solutions. To reduce the influence of shading noise and improve the subdivision positioning accuracy of demodulation, a CCD camera is used to enlarge the image for secondary imaging processing, as shown in Fig. 11, which shows noise without shading and a clear fringe image.

5.2. Experiment on static denoising of displacement images

To facilitate calculation and subsequent analysis, the original image received by the camera is too large, as shown in Fig. 12(a). It can be seen from the previous theory that high-frequency noise has a serious impact on image quality. It should be filtered first, the fringe center position should be mainly considered when denoising, and the edge part can be weakened appropriately. First, Fig. 12(a) carries out grayscale transformation to obtain a grayscale image of the original image and then uses low-pass filtering to obtain Fig. 12(b). After many experimental comparisons, 800 Hz is selected as the cut-off frequency. The image filtered by this frequency not only retains the clear contrast between stripes but also filters out the high-frequency noise of the image. Compared with the original Fig. 12(a), it can be found that the filtered gray image becomes smooth, and the gray continuity is improved. Then, we use the inverse proportional kernel NLM method designed in this paper to perform secondary denoising processing on Fig. 12(a) and obtain Fig. 12(c). Compared with Fig. 12 (b), the image denoised by the inverse ratio kernel NLM reduces more noise information and improves the image quality.

For a more visual comparison of the effect before and after image demodulation, we compare Fig. 12(a)-(c), take the gray value corresponding to the image pixel position as the longitudinal axis information, and draw the gray three-dimensional surface diagram, as shown in Fig. 13(a)-(c). Compared with Fig. 13(a) and (b), it can be seen that after

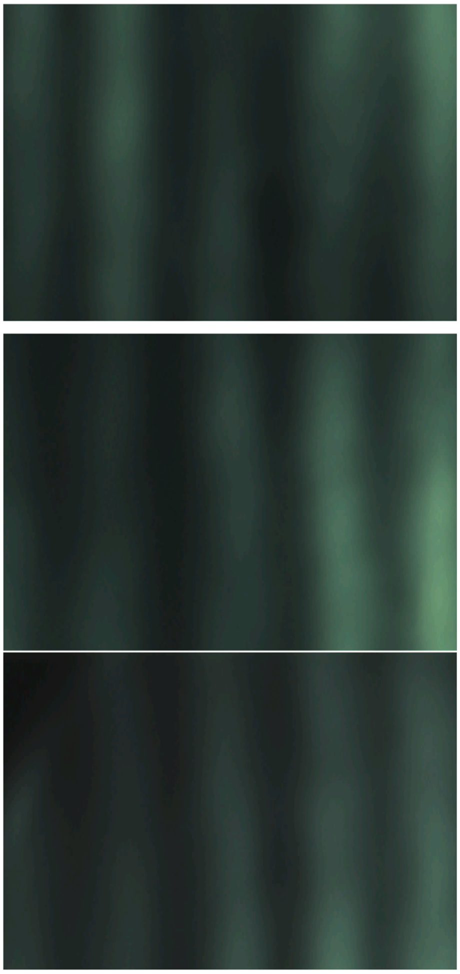

Fig. 14. Three sampled fringe images.

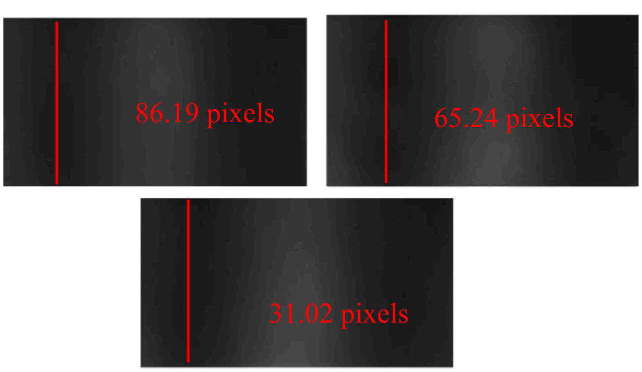

Fig. 15. Denoised gray image.

low-pass filtering, the overall surface becomes smoother, filtering most of the high-frequency noise. Comparison of Fig. 13(b) and (c), it can seen that near the image peak curve, the image denoised by the inverse ratio kernel NLM further reduces the number of jump points, and the neighborhood of the curve peak becomes smoother. Then, comparing Fig. 13 (a) and Fig. 13(c), it can be found that the image quality after denoising is significantly improved.

The high-precision displacement table was used to verify the measurement effect of the system. The high-precision displacement table was set to move forward to three positions of 20 nm, 40 nm and 60 nm, and the grating moving positioning experiment was carried out. Fringe images are captured at three static positions. After repeated experiments and debugging, the better fringe images corresponding to the three positions were obtained. As shown in Fig. 14.

The three original images are intercepted at the same position based on the center of the detection plane and are then denoised, as shown in Fig. 15.

The demodulation algorithm proposed in this paper is used to subdivide and locate the three images. The calculation results show that the sub-pixel positioning values of the first dark stripe are 86.19pixel, 65.24pixel and 31.02pixel respectively, which can realize the static sub-pixel positioning of the moving stripe image. Based on this, the positioning values of 22.7 nm, 38.2 nm and 63.3 nm of the three positions were obtained by further demodulation calculation, indicating that the nano-level positioning measurement of displacement was completed.

6. Conclusion

In this paper, an inverse nuclear NLM grating displacement interference signal demodulation measurement method was proposed and designed. By transforming the traditional photodiode detection method into a CCD image detection method, we analyze the characteristics of interference fringe imaging, and combine the characteristics of the periodic texture structure of the fringe image. Based on the traditional non-local mean (NLM) demodulation algorithm, an NLM denoising method with inverse proportional kernel function is proposed, and the effectiveness of the algorithm is verified by experiments. This algorithm plays an important role in improving image positioning accuracy and displacement measurement accuracy.

Funding

This project was supported in part by the State Key Laboratory of applied optics (No.SKLAO2021001A03); in part by the Key R & D of Jilin Provincial Department of Science and Technology-Key Industrial Core Technology Research Project (20210201091GX) and in part by the National Natural Science Foundation of China (No.62005101).

CRediT authorship contribution statement

Xu Gao: Data curation, Formal analysis, Funding acquisition, Methodology, Software, Validation, Writing – original draft. **Xuebin Zhang:** Formal analysis, Visualization, Data curation. **Kaiwei Li:** Conceptualization, Investigation, Project administration, Resources, Supervision. **Pengfei Wang:** Writing – review & editing.

Declaration of Competing Interest

The authors declare that they have no known competing financial interests or personal relationships that could have appeared to influence the work reported in this paper.

References

[1] P. Jinshan, S. Zhixun, W. Wei, Optical Flow Method for Motion Details Estimation [J], J. Computer-Aided Des. Computer Graphics, 23(08) (2011) 433-1441.
[2] S. Grossberg, E. Mingollaa, Neural dynamics of visual motion perception: local detection and global grouping[C], Neural Networks for Vision and Image Processing. Massachusetts, MIT Press, 1992, pp. 293-342.
[3] D. Serby, S. Koller-Meier, L.V. Cool, Probabilistic object tracking using multiple features [A], in: IEEE International Conference of Pattern Recognition (ICPR) [C], 2004, pp. 184-187.
[4] D. Comaniciu, V. Ramesh, P. Meer, Kernel-based object tracking, IEEE Trans. Pattern Anal. Mach. Intell. 25 (2003) 564–575.
[5] D. Ballard, C. Brown, Computer Vision [M], Prentice-Hall, 1982.
[6] B. Lucas, T. Kanade, An Iterative Image Registration Technique with an Application to Stereo Vision. Artificial Intelligence, Vancouver, Canada, Aug, 1981, pp. 674-679.
[7] B.K. Horn, B.G. Schunck, Determining Optical Flow, Artif. Intell. 17 (10) (1981) 185–203.

[8] Q. Lili, The principle research on small optical pattern rotary encoder with high resolution [D].Changchun Institute of Optics, Fine Mechanics and Physics, Graduate University of Chinese Academy of Sciences (2013).

[9] Q. Lili, W. Qiuhua, Angular measurement technology for high resolution area array image optical encoder [J], Chinese J. Sci. Instrum. 34 (01) (2013) 234–240.

[10] L. Hao, Z. Changhe, W. Shaoqing, et al., Two-dimensional gold matrix method for encoding two-dimensional optical arbitrary positions[J], Opt. Express 26 (10) (2018) 12742.

[11] X. Wenzhuo, K. Zhiyong, Z. Wei, et al., Phase correction of quartering deviation of photoelectric rotary encoder [J], Opt. Precision Eng. 15 (11) (2007) 1745–1748.

[12] Z. Niu, X. Zhang, X. Xu, et al., Compensation of nonlinear errors of phase-shifted fringes in phase measuring deflectometry[P], International Symposium on Precision Mechanical Measurements (2019).

[13] M. Zelong, T. Xiaoqi, S. Bao, et al., Research of the Tracking-loop Subdivision for Sine-cosine Encoder Signal [J], ELECTRIC DRIVE 42 (5) (2012) 50–52.

[14] Y. Hai, Q. Wan, Novel nano-scale absolute linear displacement measurement based on grating projection imaging[J], Measurement 182 (2021), 109738.

[15] X. Hai, Z. Xin, J.i. Mian, Complex Texture Region Denoising Based on BM3D Image Denoising[J], COMPUTER ENGINEERING & SOFTWARE 41 (33) (2020) 182–187.

[16] M.E. Salih, X. Zhang, M. Ding, An Improvement of Non-Local Means Denoising Method in the Presence of Large Noise [J], Applied Mechanics and Materials 2171 (2013).

[17] H. Baofei, Low frequency noise characteristics of electronic components and related testing technology [J], ELECTRONIC TEST 04 (2021) 32–34.

[18] F. Linwei, Research on image denoising based on non local mean and regularization model[D].Shandong, University, 2019.

[19] J. Duran, A. Buades, B. Coll, C. Sbert, Blanchet G.A survey of pansharpening methods with a new band-decoupled variational model [J], ISPRS J. Photogramm. Remote Sens. 125 (2017).

[20] R.D. Nowark, Wavelet based Rician noise removal for magnetic resonance imaging, IEEE Trans. Image Process. 8 (10) (1999) 1408–1419.

[21] L. Siwei, E.P. Simoncelli, Modeling multiscaIe subbands of photographic images with fields of Gaussian Scale Mixtures,“ IEEE Transactions on Pattern Analysis and Machine Intelligence, vo1. 31, no. 4, 2009, pp.693-706.